Fermi National Accelerator Laboratory

FERMILAB-Pub-92/190

Beam Test of a Parallel-Plate Calorimeter with High Pressure Gas as Active Medium

L. Demortier, N.D. Giokaris, K. Goulianos, D. Khazins

Experimental Physics Department
The Rockfeller University, New York, NY 10021

D.F. Anderson, S. Cihangir, A. Para, J. Zimmerman

Fermi National Accelerator Laboratory
P.O. Box 500, Batavia, Illinois 60510

G. Fanourakis

Department of Physics and Astronomy
University of Rochester, Rochester, NY 14627

J.A. Budagov, A.D. Volkov

Joint Institute for Nuclear Research (Dubna)
P.O. Box 79, 101000 Moscow, Russia

M. Morgan

Ability Engineering Teehnology, Inc.
South Holland, Il. 60473

July 1992

Submitted to *Nuclear Instruments and Methods A*

Operated by Universities Research Association Inc. under Contract No. DE-AC02-76CHO3000 with the United States Department of Energy

Disclaimer

FERMILAB-Pub-92/190
July 1992

BEAM TEST OF A PARALLEL-PLATE CALORIMETER WITH HIGH PRESSURE GAS AS ACTIVE MEDIUM

L. Demortier, N. D. Giokaris, K. Goulianos, D. Khazins
Experimental Physics Department, The Rockefeller University, New York, NY 10021, USA

D. F. Anderson, S. Cihangir, A. Para, J. Zimmerman
Fermi National Accelerator Laboratory, P.O. Box 500, Batavia, IL 60510, USA

G. Fanourakis
Department of Physics and Astronomy, University of Rochester, Rochester, NY 14627, USA

J. A. Budagov[1], A. D. Volkov
Joint Institute for Nuclear Research (Dubna), P.O. Box 79, 101000 Moscow, Russia

M. Morgan
Ability Engineering Technology, Inc., South Holland, IL 60473, USA

(Submitted to Nuclear Instruments and Methods A)

A prototype parallel-plate electromagnetic calorimeter, using high pressure gas as active medium, has been tested in an electron beam at Fermilab. Data were taken in the pressure range of 20 to 100 atm, and with incident beam energies ranging from 16 to 125 GeV. Results on the calorimeter response as a function of electric field, gas pressure, and beam energy are presented for pure argon gas and for several argon-methane mixtures. The calorimeter proved easy to operate, and fast signals were obtained with the argon-methane gas.

1. Introduction

Ionization calorimeters using high pressure gas as the sampling medium offer several advantages over other types of calorimetry. Their unity gain and relatively high energy

[1]also INFN, Pisa, I-56010 Pisa

sampling fraction eliminate the fluctuations in energy measurement observed in proportional chamber calorimeters due to electron multiplication and variations in atmospheric pressure, and greatly suppress the occurrence of "Texas Towers" [1], which are caused by slow moving neutrons scattered off protons. The technique is relatively insensitive to impurities, in contrast with warm liquid calorimetry. It does not require cryogenics, and can withstand the radiation expected in the forward region of SSC detectors (about 10 Mrad per year at a polar angle of 1.5°, 12.5m away from the interaction point). Finally, the signal is fast enough to suit calorimetry in the high interaction rate environment of the new generation of colliders.

Some of these characteristics of high-pressure gas calorimeters were substantiated in an earlier paper [2]. The construction and testing of actual prototype calorimeters at 20 atm [3, 4, 5], have corroborated the feasibility of this technology. This paper describes a calorimeter designed to operate at up to 100 atm gas pressure. Higher pressures improve the signal to noise ratio and further suppress the rate of "Texas Towers". The main objectives of our study were to prove that a calorimeter can be built and safely operated at 100 atm, measure the effect of CH_4 concentration on signal size and speed, compare the response of the calorimeter for different gas mixtures, select the best mixture and, finally, measure the energy resolution and compare it with expectations. The following sections describe the calorimeter construction and testbeam setup, as well as data acquisition and analysis.

2. Calorimeter construction

The prototype calorimeter consists of ten sampling layers, each of which is a high pressure vessel made up of two parallel steel disks bolted together (see figure 1). The disks have an outside diameter of 28.6 cm and are approximately 3.0 cm thick, making the assembled calorimeter about 30 radiation lengths long. A 21.2 cm diameter, 5.5 mm deep recess is milled in one of the two disks that constitute a vessel. Halfway inside this recess, a 1.5 mm thick G10 readout board is supported with ceramic spacers. Two copper pads are etched on each side of the board: a 17.8 cm diameter pad to collect the charge from electron showers and a 3.2 cm diameter pad for muons. Small holes through the board serve to establish electrical contact between the two electron pads and between the two muon pads. High pressure gas occupies a 2 mm gap on each side of the G10 board. When the device is operated, the pads are brought to a positive high voltage and collect the charge deposited in the cavity they are facing. The gas is supplied through a valve mounted in a special port drilled on the side of one disk. A second valve provides a 101 atm relief. Three out of the ten vessels have an ^{241}Am α-source mounted in front of the muon pad. These sources were used to monitor the gas. The signal produced by ionization of the gas is carried from the collection pads to external amplifiers through high voltage, high pressure feedthroughs. To minimize the source capacitance, these amplifiers were mounted as close to the feedthroughs as possible.

3. Testbeam setup

The calorimeter was tested in the Fermilab NT beam line towards the end of the 1991 fixed target run. Two types of current amplifiers were used for this test. Some of their parameter values, as measured by us in bench tests, are listed in Table 1. The amplifier

Table 1: Characteristics of the amplifiers used in the testbeam.

Parameter	Amplifier 1 [6]	Amplifier 2 [7]
Output signal rise-time (0.1 to 0.9 levels)	5 ns	10 ns
Output signal decay-time (0.9 to 0.1 levels)	15 ns	10 ns
Input impedance	214 Ω	63 Ω
Effective r.m.s. current noise i_{noise}	3.2 $pA/\sqrt{Hz}$	3.8 $pA/\sqrt{Hz}$
Effective r.m.s. voltage noise	0.73 $nV/\sqrt{Hz}$	0.62 $nV/\sqrt{Hz}$
Gain	32 $mV/\mu A$	11 $mV/\mu A$

outputs were connected through 120 m long cables to a LeCroy 2280 CAMAC ADC system, which was read out by a MAC II computer through a GPIB interface. No signal shaping was done.

Most of the measurements described in this paper were performed with amplifier 1. Its output pulse exhibited a long tail because of its large input impedance and because of the relatively large electrical capacitance of the vessels ($\approx$ 230pF). A gate of 260 ns width was used to collect the electron charge deposited in the gas gaps. This gate was long enough to accomodate a large variety of run conditions. On the other hand, the output signal from amplifier 2 was very close to the expected triangular current pulse from the detector (fig. 2). This amplifier was only used for a few runs with 95%Ar+ 5%CH_4 at 100 atm. Here, a gate width of 60 ns was selected. We estimate that about 13% of the signal was lost in this case.

4. Data acquisition

Our trigger was BEAM $\cdot$ T1 $\cdot$ TRD $\cdot$ $\overline{T2}$, where BEAM is a beam-defining, upstream set of scintillation counters, T1 is a 2.54 $\times$ 2.54 cm^2 scintillation counter right in front of the calorimeter, TRD is a transition-radiation detector used to identify electrons, and T2 is a 10 $\times$ 10 cm^2 scintillation counter placed behind the calorimeter and used to reject punch-through hadrons that triggered the TRD. This trigger resulted in very clean electron samples at 16 and 50 GeV. However, a small fraction of pions contaminated our samples at higher energies. See figure 3, which shows some typical pulse height spectra.

Pedestal events were collected during each data-taking run, between consecutive beam spills. The trigger was provided by a pulser. The widths of the measured pedestal peaks can be compared with the total amplifier r.m.s. noise charge Q_{noise} calculated according to the equation:

$$Q_{noise} = i_{noise} \cdot \sqrt{\frac{T}{2}} \cdot \sqrt{n} \qquad (1)$$

where i_{noise} is the effective r.m.s. current noise, T the gate width, and n the number of calorimeter vessels used. The result of the comparison is shown in table 2. Calculated and measured values of the calorimeter noise do not differ much and are close to 0.8 GeV.

Table 2: Amplifier noise calculation versus measured pedestal width

Parameter	Amplifier 1	Amplifier 2
Gate width T	260 ns	60 ns
Calculated r.m.s. noise charge Q_{noise}	3.6 fC	1.9 fC
Equivalent calorimeter energy	0.95 GeV	0.52 GeV
Measured pedestal width	0.87 GeV	0.74 GeV

Electronic calibration was performed by injecting a pulse of known current, and with a width similar to that observed from beam particles, at the input of each amplifier. These data provide the absolute charge calibration and the relative channel-to-channel calibration.

We took data with a variety of gas mixtures, pressures, and high voltages. For this reason, it was important to monitor the stability of the calorimeter under a standard set of run conditions. These standard run conditions were 50 GeV electrons, a gas mixture of 95%Ar+ 5%CH_4 at 100 atm, and a cell high voltage of 1500 V. Figure 4 shows the calorimeter response under these conditions, as a function of time. The straight line is a fit to the data points. The calorimeter response was stable at the 1% level during the run. In the next section we will describe the data obtained from pure argon gas and several argon–methane mixtures. Other gases ($Ar + CF_4, Ar + C_2H_6, Xe + CH_4$) were also studied. Results from those studies will be presented in a forthcoming publication.

5. Data analysis and results

Data analysis proceeds as follows. For a given run, channel pedestals are computed by averaging the channel pulseheights over all the pedestal events in the run. For each beam event in the same run, these pedestals are subtracted from the corresponding channel pulseheights. The results are then multiplied by individual channel calibration factors which convert ADC counts into charges. Finally, a small correction factor is applied to compensate for the loss of pressure due to gas leakage during a run. This correction is typically of the order of a few percent. It is computed by linear interpolation between gas pressure measurements performed before and after each run. Since we recorded the time of occurrence of each event, it is possible to apply the pressure correction on an event by event basis. The sum of the ten electron channels is subsequently formed, and the mean and width of the corresponding distribution are extracted by fitting with a gaussian. A double gaussian fit is used wherever the pion contamination is significant, especially at the higher energies. Since we did not measure the incident electron momentum for each event, we correct the width of the electron peak by subtracting the beam momentum bite in quadrature. This bite is estimated to be $(2.5 \pm 0.5)\%$. We similarly correct the width of the electron peak for electronic noise, by subtracting in quadrature the pedestal width.

Figure 5 shows the charge collected in the calorimeter as a function of the high voltage across the 2 mm gas gaps, for 100 atm and 50 GeV electrons. The signal saturates at the comfortable electric field of about 500 V/mm (our standard high voltage setting was 1.5 kV).

The dependence of the calorimeter response on pressure is presented in figure 6. Three effects can spoil the linearity of this dependence. First, the gas density does not vary linearly with pressure because of Van der Waals forces. This effect increases the signal by 8% at 100 atm. Next, electron-ion recombination reduces the signal by about 8% (see below). Finally, as the gas pressure increases, a smaller number of the low energy shower particles originating in the steel plates will be able to cross the entire width of the gas gaps. The energy deposited by these particles will no longer increase with pressure. Hence the total energy deposited in the gaps grows less rapidly than what is expected on account of gas density alone. This effect is shown by the curve superimposed on the data points in figure 6. The curve is the result of an EGS4 Monte Carlo simulation [8] with a kinetic energy cut-off of 200 keV on both electrons and photons. This simulation does not include the effect of Van der Waals forces nor that of charge recombination.

The linear dependence of the calorimeter signal amplitude on beam energy is demonstrated in figure 7. A fit through all the data points yields a calorimeter response of (3.8 ± 0.4) fC/GeV, where the error reflects our uncertainty in the electronic calibration. This figure is to be compared with a calculated value of 4.5 fC/GeV. The calculation is based on a e/μ ratio of 0.92 [9], and on an energy sampling fraction of 0.17%, in which we have taken into account the effect of Van der Waals forces on the gas density. The difference between measured and calculated values can be explained as the effect of recombination.

The energy resolution is plotted versus $1/\sqrt{E_{beam}}$ in figure 8. Again, a linear relationship is observed. Fitting the data to an energy resolution function of the form $A/\sqrt{E}$, we obtain $A = (44.3 \pm 0.2)\%$. This agrees with EGS4 calculations, which give $A = (45 \pm 1)\%$. The energy resolution is expected to improve with increasing pressure, since the total track length of soft particles in the gas regions, and hence fluctuations in this track length, diminishes as the gas becomes denser. Figure 9 shows the variation of the energy resolution with gas pressure. The data are seen to agree with EGS4.

The effect of methane concentration has also been studied. Adding methane lowers the gas density and increases electron–ion recombination [2]; both effects tend to reduce the amount of charge collected in the gas gaps, as evidenced by figure 10. The straight line in that plot shows the change in calorimeter signal expected from the decrease in gas density alone. For a 5% methane concentration, the effect of recombination is about 8%. On the other hand, the energy resolution is essentially insensitive to methane concentration (see figure 11). Finally, the large methane molecules also cool the drifting electrons, dramatically improving the collection time. The collection time of electrons in 95%Ar + 5%CH_4 at 100 atm has been measured to be about 20 ns/mm, in agreement with previous work [10, 2]. This should be compared to 380 ns/mm in pure argon gas at the same pressure [2].

6. Conclusions

A high pressure gas calorimeter has been constructed and tested in the pressure range of 20 to 100 atm. It proved easy to operate and its response was very stable over the run period. The collected signal saturates at the comfortable electric field of 500 V/mm and scales linearly with incident beam energy between 16 and 125 GeV. The pressure dependence of the collected charge and the energy resolution agrees well with EGS4 predictions, proving that the behaviour of this type of calorimeter is well understood. The electron collection time in 95%Ar + 5%CH_4 at 100 atm is 20 ns/mm, which yields a signal duration comparable to that from scintillator-based calorimeters.

The parallel-plate geometry of our prototype is not practical for large surface calorimeters. However, one can build such calorimeters out of high pressure gas tubes. Our group has designed and is now constructing a prototype tube calorimeter. The speed of high pressure gas calorimeters, combined with their unity gain and inherent radiation hardness, makes them a very attractive candidate for detectors at the new high energy, high luminosity colliders (SSC, LHC), and especially for the forward region of these detectors.

Acknowledgments

This work was partly supported by the Texas National Research Laboratory Commission under Grant No. RGFY9160. We would like to thank Carlos Hojvat, Romesh Sood and Regina Rameika of the Fermilab Research Division for helping us with test-beam preparation. Thanks are also due to Hans Kobrak and Xiaorong Shi for offering us Xe gas to operate the TRD.

References

[1] S. Cihangir et al., IEEE Trans. Nucl. Sci. NS-36 (1989) 347.

[2] N.D. Giokaris et al., Nucl. Instr. and Meth. A291 (1990) 552.

[3] V.I. Baskakov et al., Nucl. Instr. and Meth. 159 (1979) 83.

[4] D.M. Khazins et al., Nucl. Instr. and Meth. A300 (1991) 281.

[5] T.A. Amatuni et al., Nucl. Instr. and Meth. 203 (1982) 179.

[6] V.M. Golovin et al., Preprint IFVE-89-231 (1989).

[7] A.D. Volkov, JINR, Dubna (1991) unpublished.

[8] W.R. Nelson, H. Hirayama, D.W.O. Rogers, SLAC-Report-265 (1985).

[9] R. Wigmans, Nucl. Instr. and Meth. A259 (1987) 389.

[10] G. Niculescu, Diploma thesis, Bucharest University, 1991 (unpublished).

List of Figures

Figure 1: Prototype parallel plate electromagnetic calorimeter.

Figure 2: Output signal from amplifier 2, for 50 GeV electrons, a gas mixture of $95\%\mathrm{Ar} + 5\%\mathrm{CH_4}$ at 100 atm, and an electric field of 750 V/mm.

Figure 3: Pulse height spectra for the four beam energies.

Figure 4: Calorimeter response under standard run conditions, as a function of time. The straight line is a fit to the data.

Figure 5: Charge collected in the calorimeter, versus the high voltage across the 2 mm gas gaps. The curve is a fit of an exponential function to the data.

Figure 6: Collected charge, normalized to gas pressure, versus pressure.

Figure 7: Collected charge over beam energy, as a function of beam energy. The straight line is a fit to the data (see text).

Figure 8: Energy resolution versus pressure.

Figure 9: Energy resolution as a function of $1/\sqrt{E_{beam}}$, where E_{beam} is the incident beam energy. The straight line is a fit to the data (see text).

Figure 10: Measured charge as a function of methane concentration.

Figure 11: Energy resolution as a function of methane concentration. The straight line is a fit to the data.

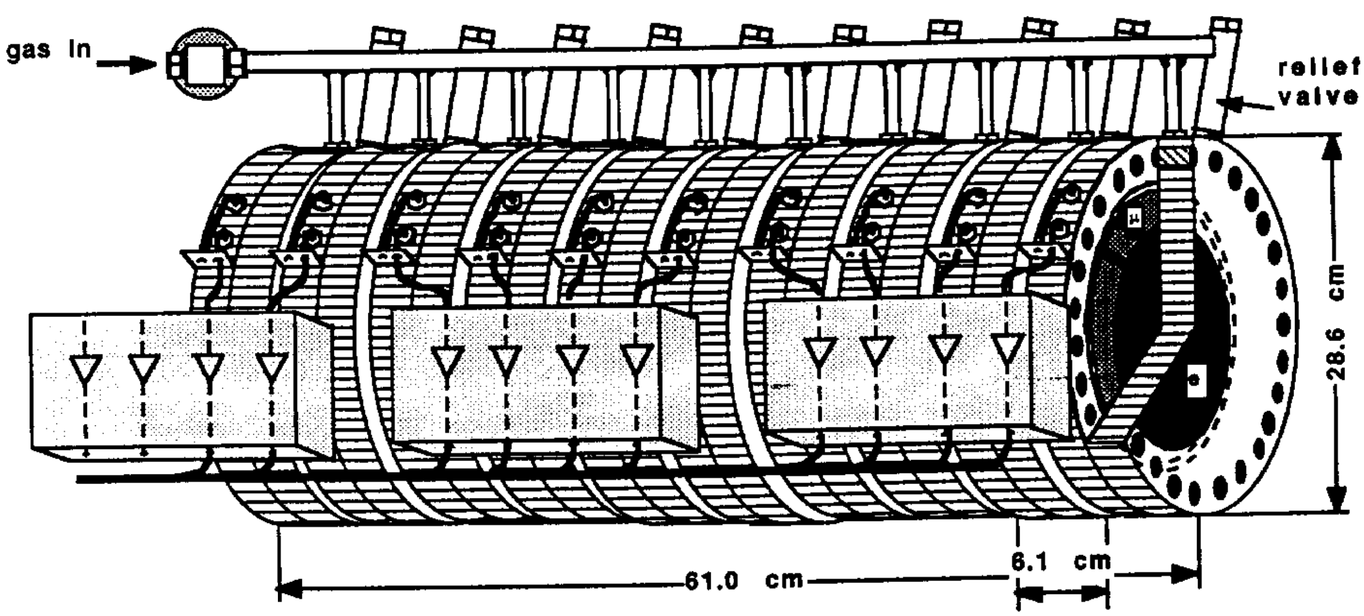

Figure 1

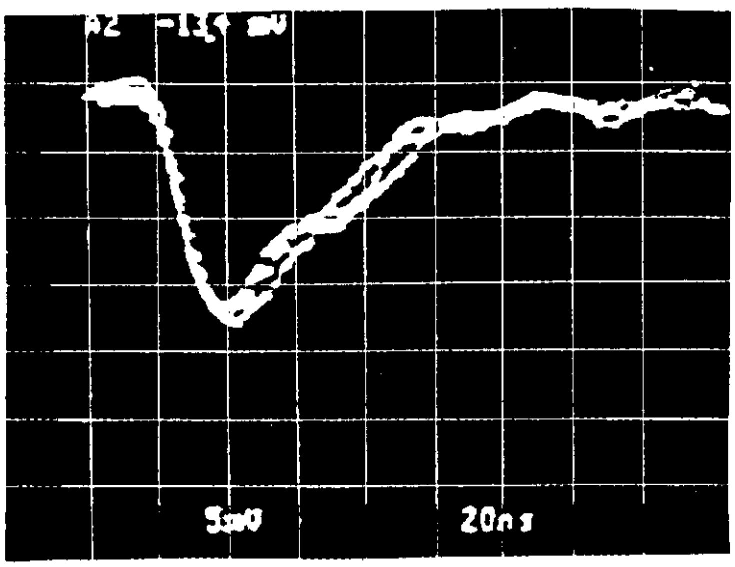

Figure 2

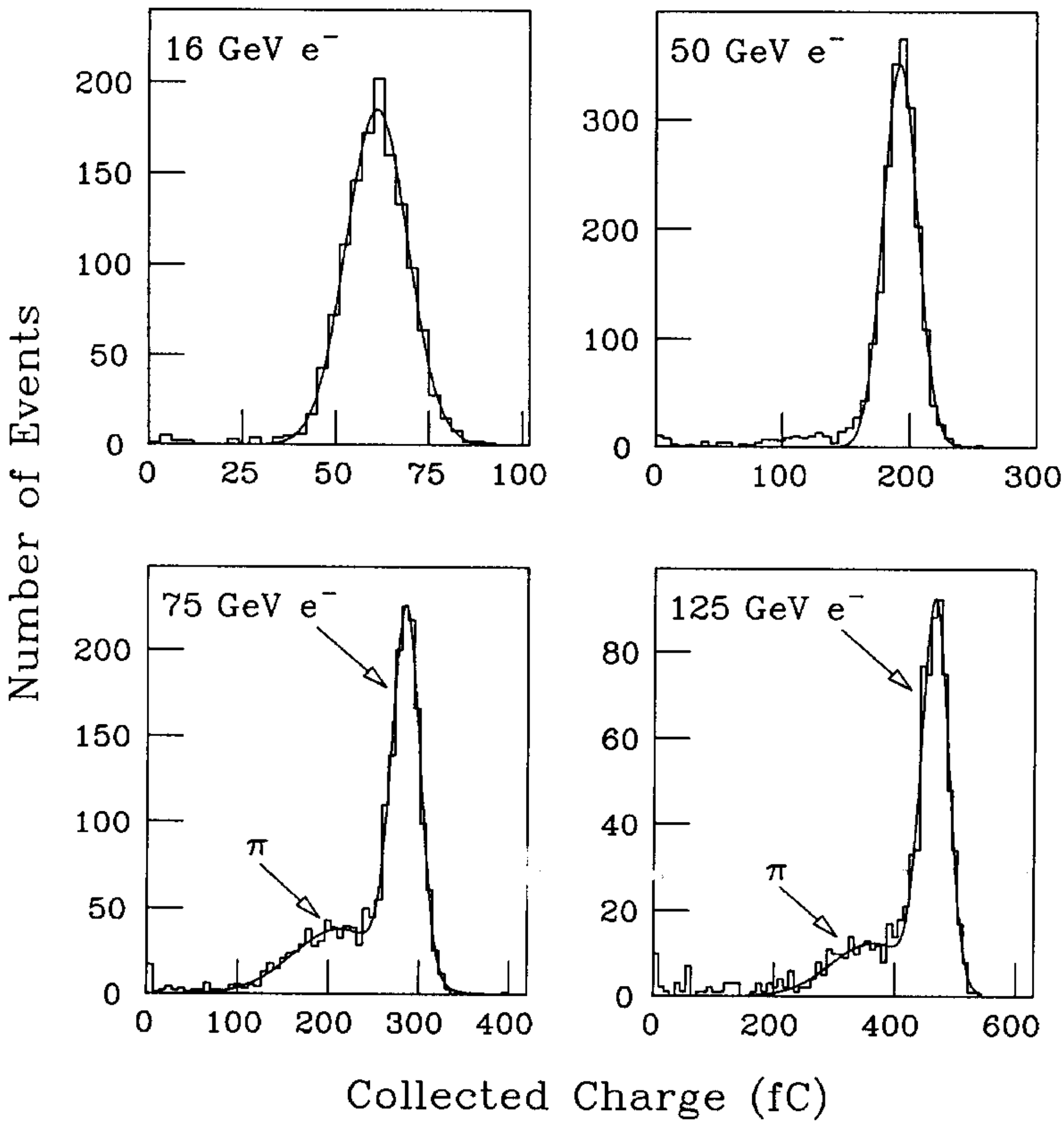
16 GeV e⁻
50 GeV e⁻
75 GeV e⁻
125 GeV e⁻
π
π
Number of Events
Collected Charge (fC)

Figure 3

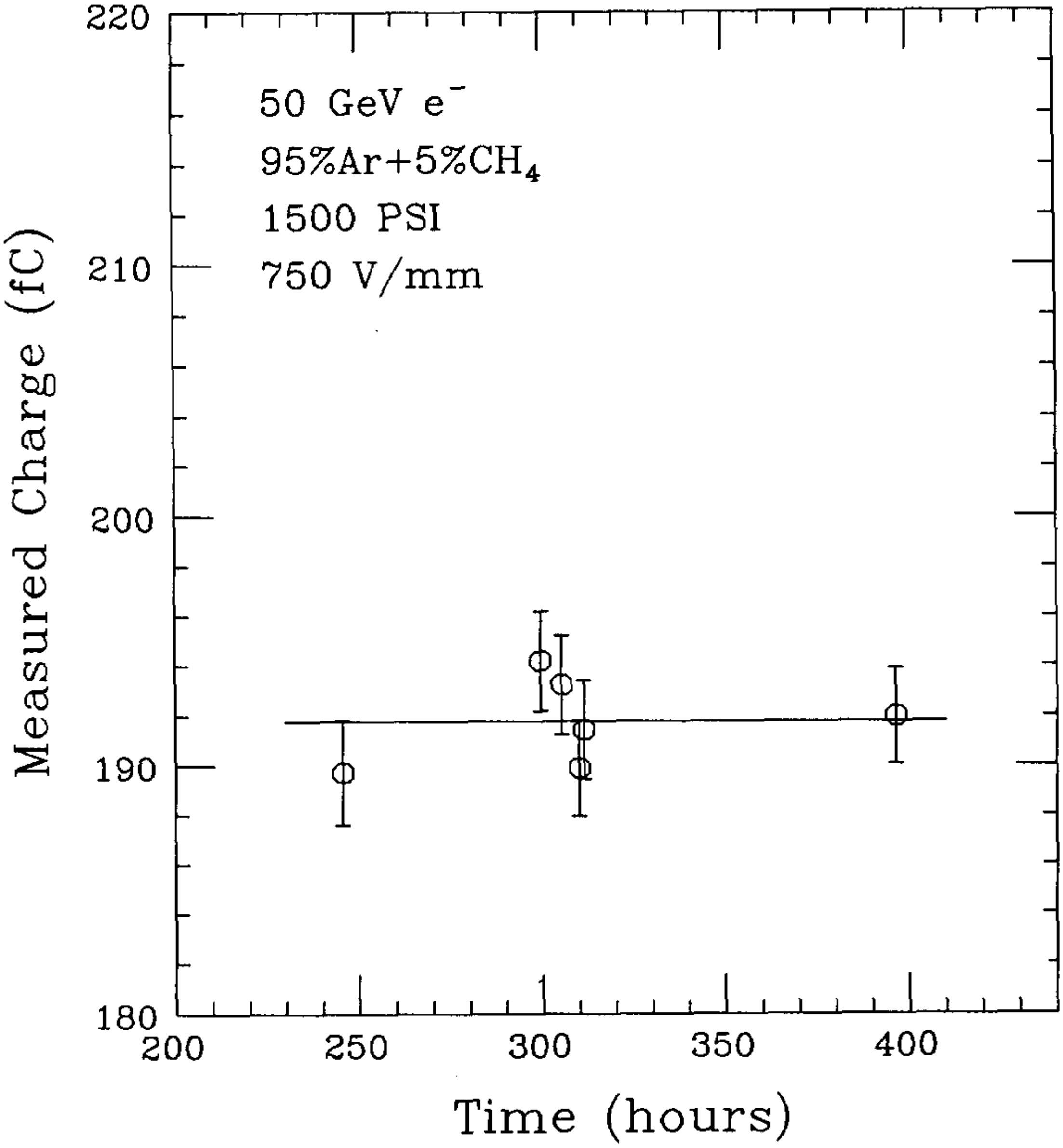
50 GeV e^-
95%Ar+5%CH_4
1500 PSI
750 V/mm
Measured Charge (fC)
Time (hours)
220
210
200
190
180
200
250
300
350
400

Figure 4

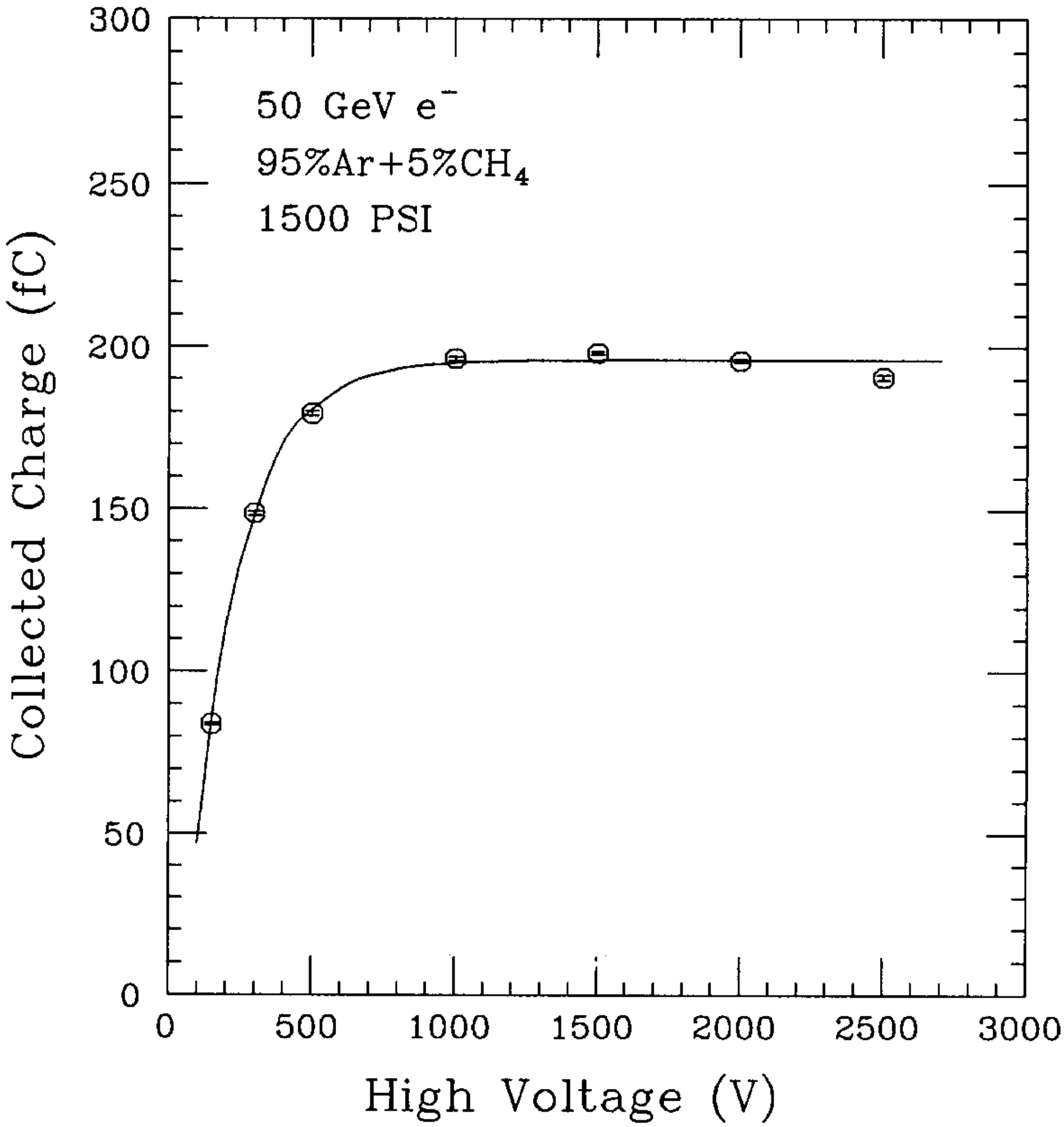

50 GeV e⁻
95%Ar+5%CH4
1500 PSI
Collected Charge (fC)
High Voltage (V)
0
50
100
150
200
250
300
0
500
1000
1500
2000
2500
3000

Figure 5

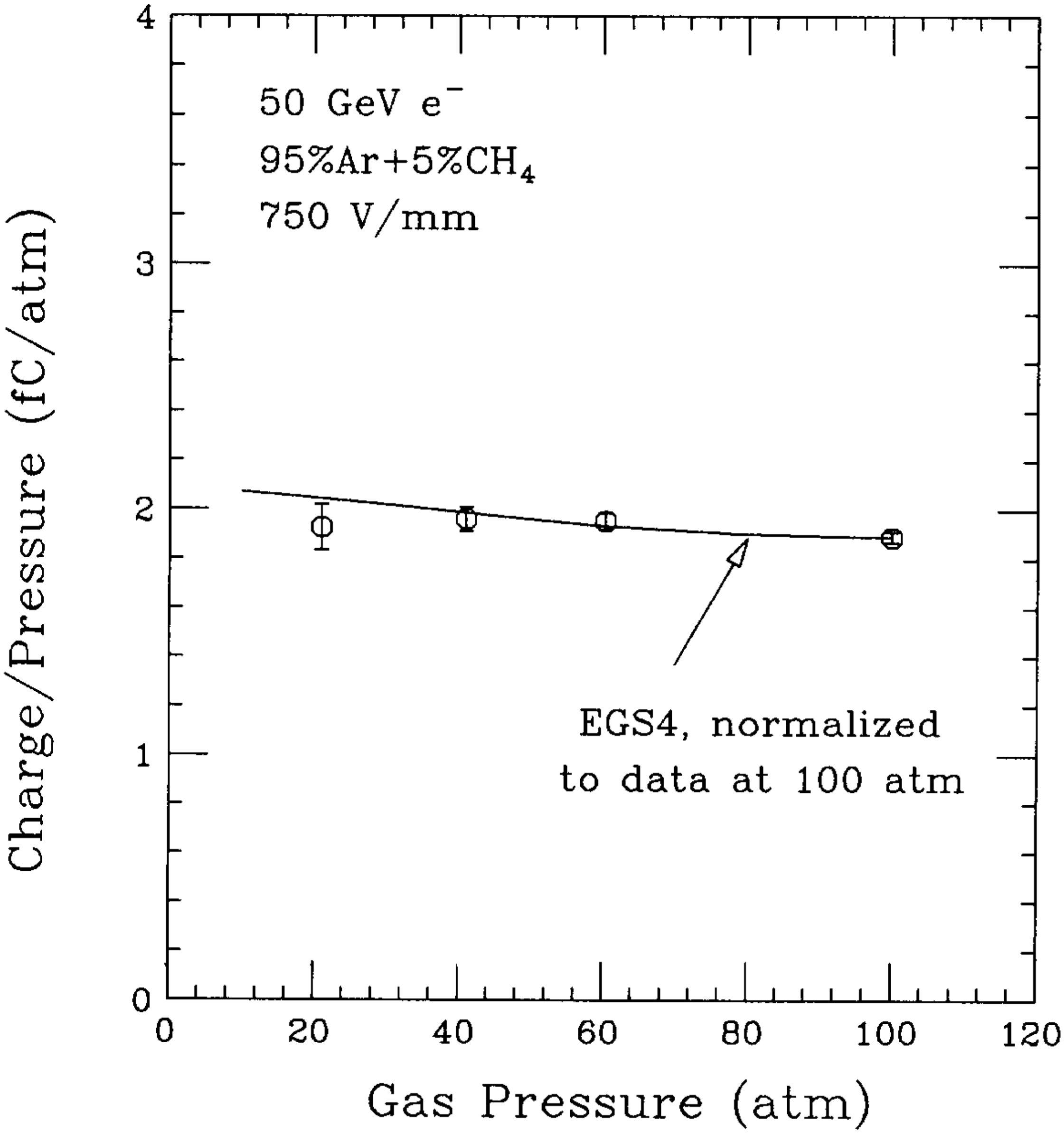

50 GeV e⁻
95%Ar+5%CH4
750 V/mm
EGS4, normalized
to data at 100 atm
Charge/Pressure (fC/atm)
Gas Pressure (atm)
0
1
2
3
4
0
20
40
60
80
100
120

Figure 6

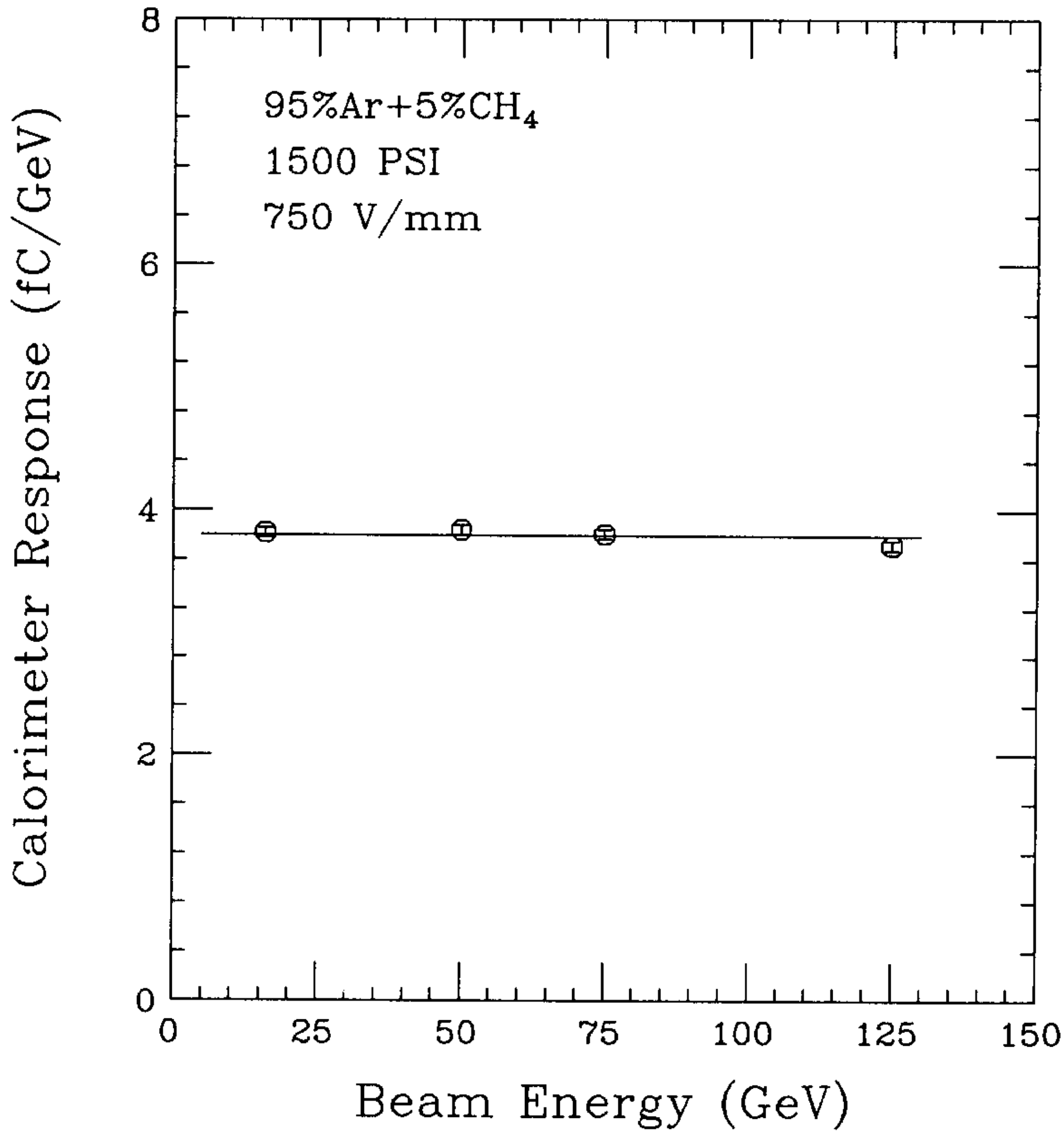
95%Ar+5%CH4
1500 PSI
750 V/mm
Calorimeter Response (fC/GeV)
Beam Energy (GeV)
0
2
4
6
8
0
25
50
75
100
125
150

Figure 7

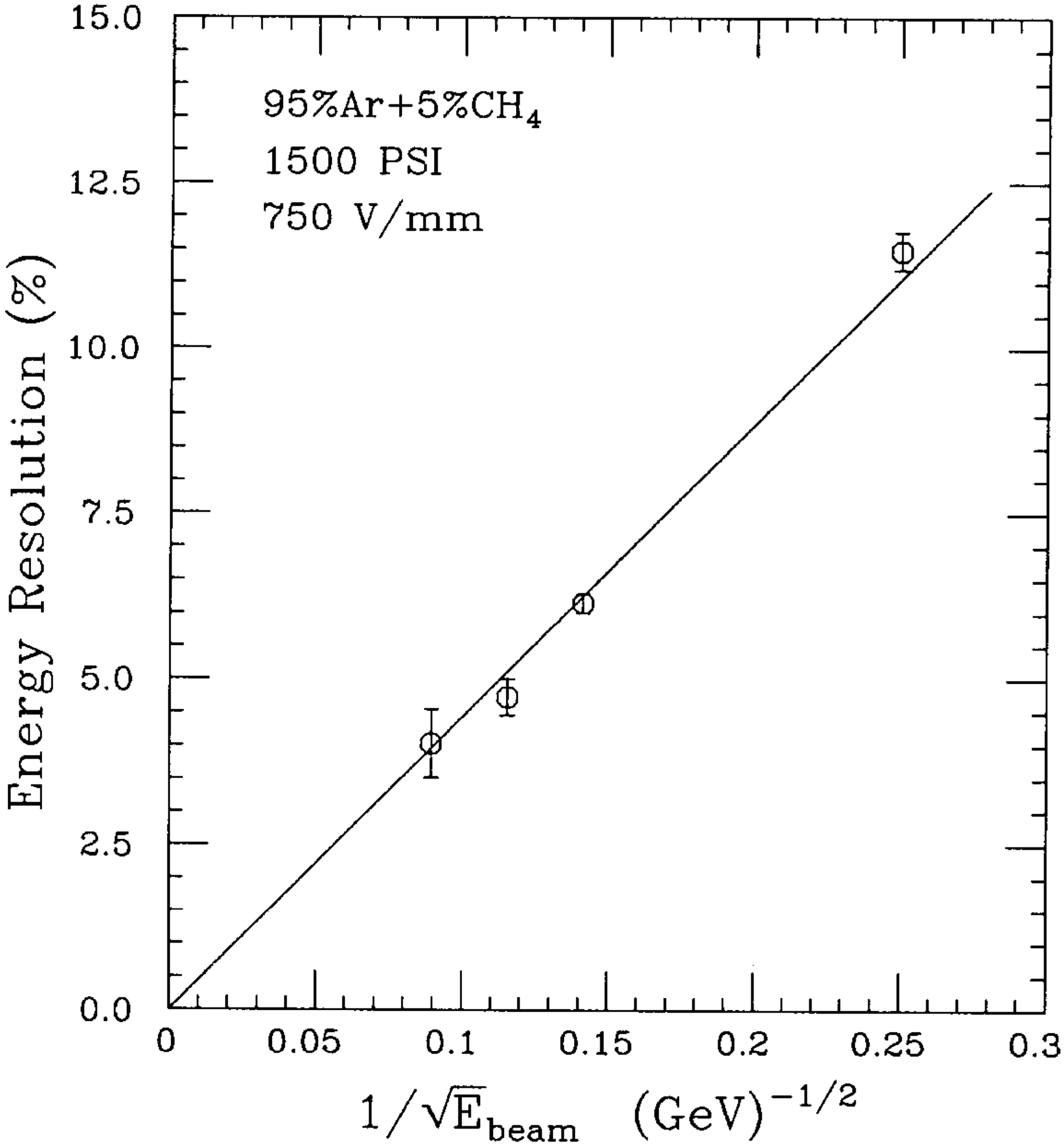
95%Ar+5%CH4
1500 PSI
750 V/mm
Energy Resolution (%)
15.0
12.5
10.0
7.5
5.0
2.5
0.0
0
0.05
0.1
0.15
0.2
0.25
0.3
1/√E beam (GeV)^-1/2

Figure 8

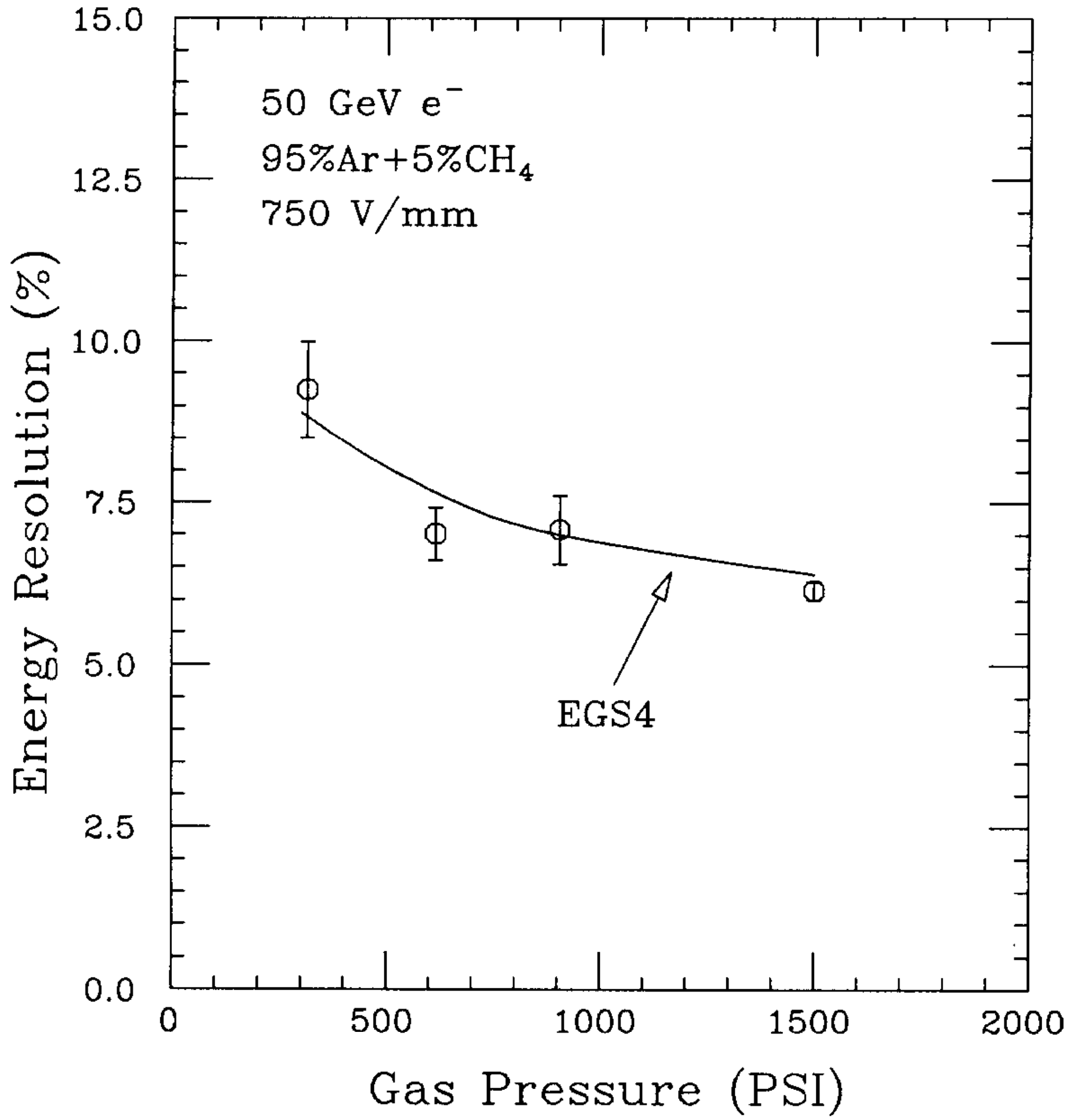

50 GeV e⁻
95%Ar+5%CH4
750 V/mm
EGS4
15.0
12.5
10.0
7.5
5.0
2.5
0.0
0
500
1000
1500
2000
Energy Resolution (%)
Gas Pressure (PSI)

Figure 9

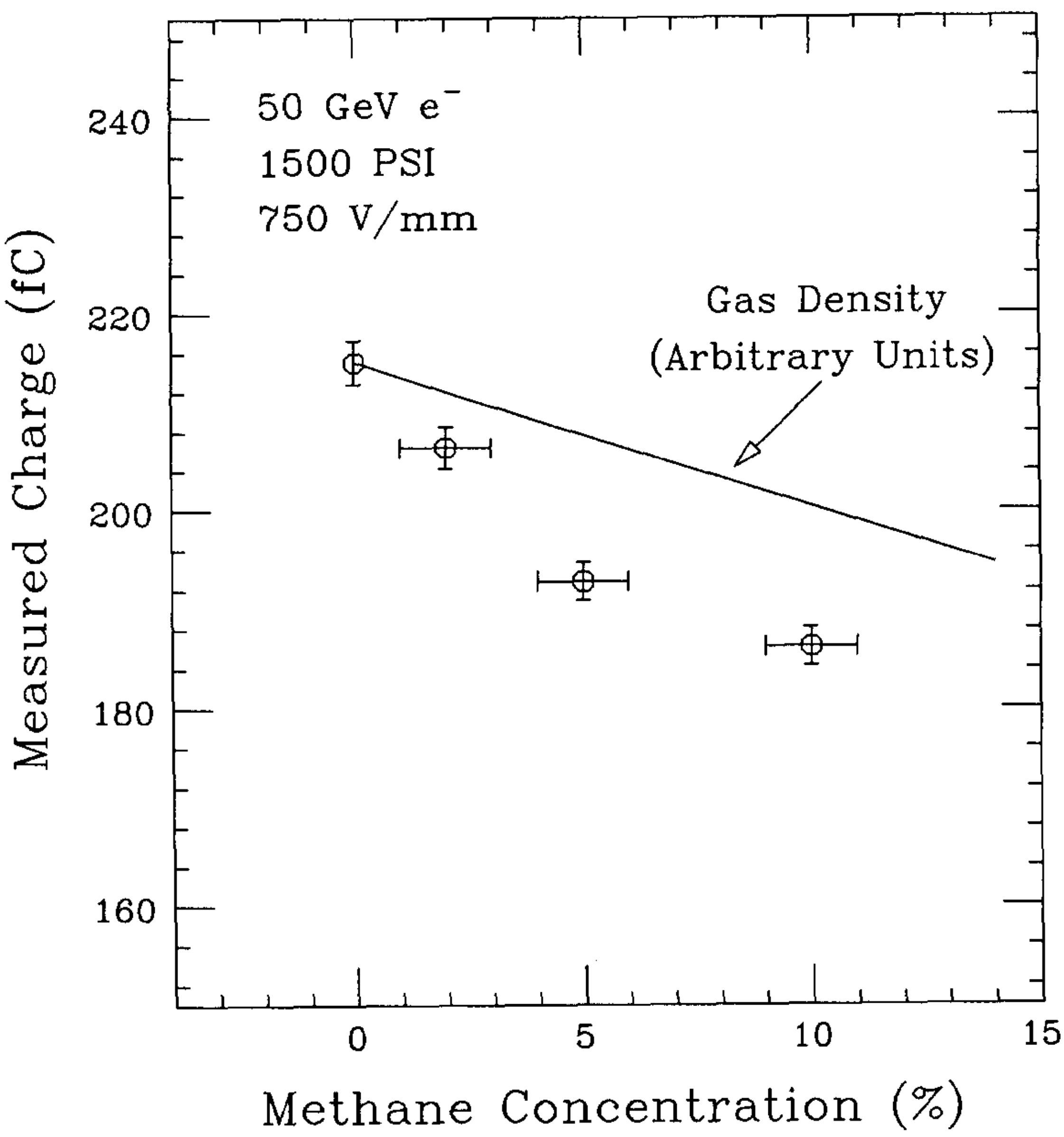
50 GeV e⁻
1500 PSI
750 V/mm
Gas Density
(Arbitrary Units)
Measured Charge (fC)
240
220
200
180
160
0
5
10
15
Methane Concentration (%)

Figure 10

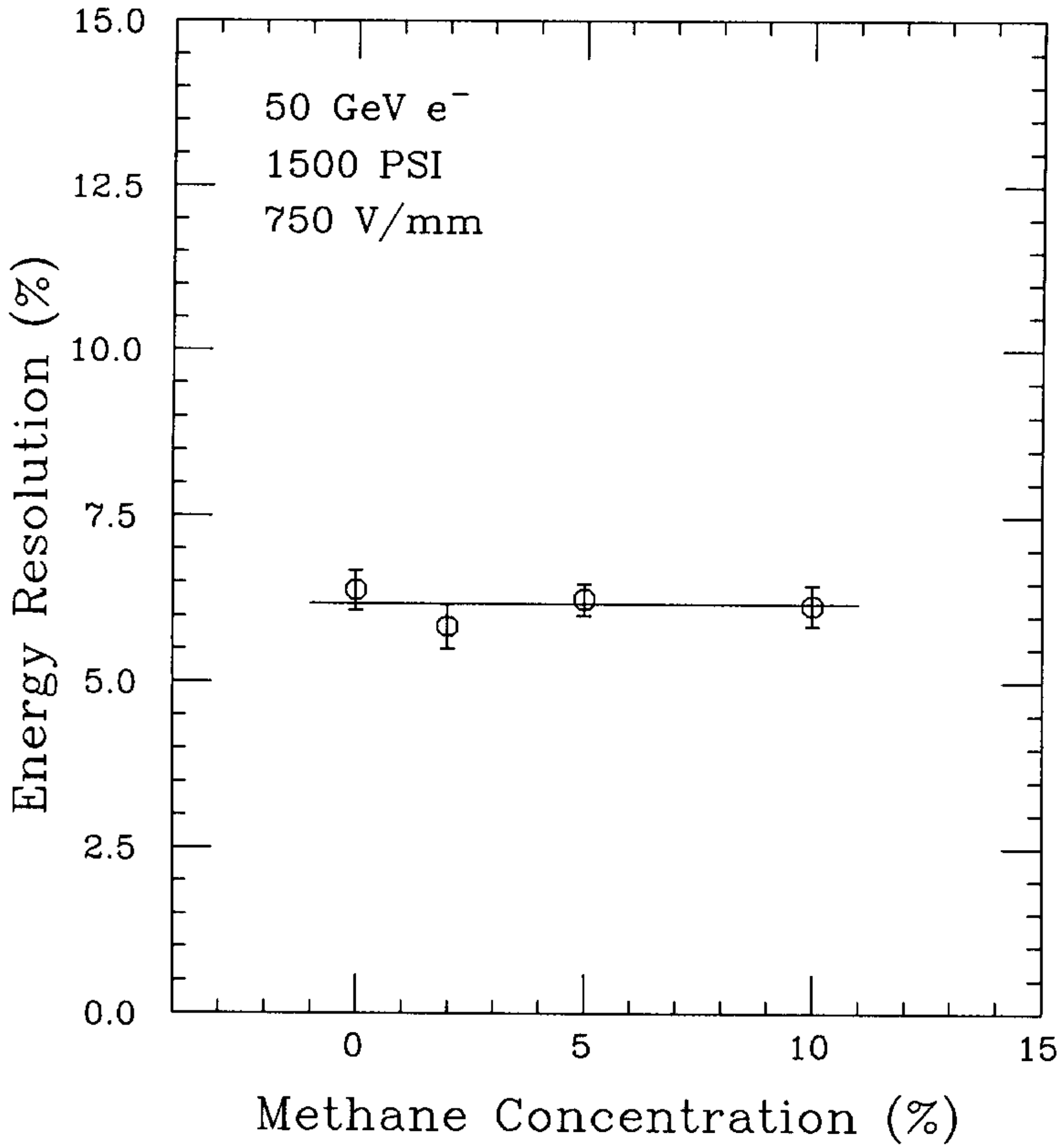
50 GeV e⁻
1500 PSI
750 V/mm
Energy Resolution (%)
15.0
12.5
10.0
7.5
5.0
2.5
0.0
0
5
10
15
Methane Concentration (%)

Figure 11